RSC Advances

ROYAL SOCIETY OF CHEMISTRY

www.rsc.org/advances

Cite this: DOI: 10.1039/c0xx00000x

www.rsc.org/xxxxxx

ARTICLE TYPE

Polymer based Nanoformulation of Methylglyoxal as an Antimicrobial Agent: Efficacy against Resistant Bacteria

Srabanti Ghosh[a†]*, Prabal Chakraborty[b], Partha Saha[b], Somobrata Acharya[a], Manju Ray[a,c]*

Received (in XXX, XXX) Xth XXXXXXXXX 20XX, Accepted Xth XXXXXXXXX 20XX

DOI: 10.1039/b000000x

Bacterial resistance to antibiotics is a severe health crisis across the globe and in the present scenario, nanoscale materials have emerged as efficient antimicrobial agents. Silver nanoparticles are well-established antibacterial agents but detrimental to eukaryotes through cytotoxicity and genotoxicity. An alternative, bioactive normal meabolite, methylglyoxal (MG) possess superior antimicrobial activity but due to the instability in air and strong enzyme induced degradation limits its application. To circumvent this emerging problem, we have developed a green strategy of using multivalent, biodegradable polymers, namely chitosan and dendrimer for the facile preparation of conjugated nanoformulations (NMG & DMG) of methylglyoxal as antimicrobial agent against resistant bacteria. Interestingly, nanoformulated methylglyoxal selectively molests the bacterial pathogens while remain biocompatible to the mammalian cells as reflected in therapeutic index. The functional group, cationic charge and nanodimension of methylglyoxal allow them to attach to and insert into membrane bilayers of bacteria and could be the defining mechanisms of antimicrobial activity. This scalable approach of the fabrication of biocompatible nanoformulated methylglyoxal with desired selectivity can revolutionize the treatment of bacterial infection minimizing the human health and environment risks.

Introduction

Invasive bacterial infection due to multidrug resistance is a major cause of morbidity and mortality in immuno-compromised patients as consequences of various medical conditions such as cancer, solid organ and stem cell transplantation, intensified chemotherapy, human immunodeficiency virus (HIV) infection or acquired immunodeficiency syndrome (AIDS).[1-3] Moreover, multi-drug resistant human pathogenic bacteria - for example, methicillin-resistant *Staphylococcus aureus* and multidrug-resistant *Pseudomonas aeruginosa* can persist as well as multiply in moist environments, such as humidifiers in hospital wards, bathrooms and kitchens which cause different types of infections.[4-9] However, most of the conventional antibacterial drugs are associate with undesirable cellular toxicity, environmental pollution with high cost and even appear insufficient to adequately combat bacterial infections.[10, 11] The discovery and development of novel antibacterial agents against resistant pathogens have extremely challenging to the pharmaceutical industry. In the present scenario, nanoscale materials have emerged as efficient antimicrobial agents owing to multimodal mechanism including silver nanoparticle, titanium oxide nanoparticles and carbon nanotubes etc.[12-14] Silver nanoparticles are well-established antibacterial agents but detrimental to human cells as well[14-16] and efforts have been made to reduce toxicity by modulating the composition, shape, size and surface coating of the nanoparticles. To circumvent this emerging problem, an alternative, bioactive normal meabolite, methylglyoxal (MG) possess superior antimicrobial activity but due to the instability in air and strong enzyme induced degradation limits its application.[17] In view of environmental and ecological safety, the importance of MG for biological response is widely recognized but due to the presence of strong and ubiquitous enzymes in human body diminishes the efficacy of MG.[17-21] We have developed an effective way of using multivalent, biodegradable polymers, for conjugated nanoformulations of MG in order to enhance its stability, carrier capacity, and targeted delivery which will effectively kill only targeted cells or microorganisms without affecting normal healthy cells. In this context, water-soluble polymer nanoconjugates are ideal for drug delivery and the use of biocompatible and biodegradable polymers such as chitosan offers promising technique for enhancing the efficacy of some existing antimicrobial agents by reducing the residual toxicity with selectivity.[22-25] Chitosan is a second-most abundant biopolymer having excellent biological properties and wound-

[a]*Centre for Advanced Materials, Indian Association for the Cultivation of Science, Kolkata-700032, India. Email:*

[b]*Crystallography and Molecular Biology Division, Saha Institute of Nuclear Physics, Kolkata-700064, India.*

[c]*Division of Molecular Medicine, Bose Institute, Kolkata 700 054, India.*

**Corresponding Author, E-mail: ghosh.srabanti@gmail.com, manju.ray.iacs@gmail.com*

[†]*Present address: Laboratoire de Chimie Physique, UMR 8000-CNRS, Bât. 349, Université Paris-Sud, 91405 Orsay, France*

†Electronic Supplementary Information (ESI) available: Additional discussions, TEM images. See DOI: 10.1039/b000000x/

healing activities.[24,25] However, the application of chitosan is limited due to its insolubility and alternatively, multifunctional PAMAM dendrimer has been utilized for the encapsulation of methylglyoxal. The dendrimer molecules are small enough to pass into the cell membrane and can be used to deliver substances such as drugs, genetic materials as well as chemical markers right into the cells in order to couple high cellular uptake and target specificity.[26-30]

Hence, our aim is to develop polymer conjugated nanoformulated MG as a potent antibacterial material under ambient conditions for biomedical applications. Here, we report for the first time a new straightforward approach for the polymer conjugated MG based nanoformulations (NMG and DMG) with superior inhibitory ability towards bacterial growth through controlled release to achieve desired bactericidal or bacteriostatic effects with minimal eukaryotic toxicity. The antimicrobial activity of nanoformulations have been tested against four clinically significant micro-organisms-gram negative bacteria such as *Escherichia coli* (*E. coli*), *Pseudomonas aeruginosa* (*P. aeruginosa*) and gram positive bacteria such as *Staphylococcus aureus* (*S. aureus*), *Bacillus subtilis* (*B. subtilis*), suggests the promising environment friendly applications of these low-cost and highly effective polymer conjugated MG. In order to understand the mechanistic pathway, the microscopic techniques have been used to study morphological changes of the cells after NMG treatment. The possibility of superoxide anion ($O_2^{\bullet-}$) induced reactive oxygen species (ROS) production has been evaluated. To the best of our knowledge, no prior study on the antimicrobial activity of polymer based nanoformulation of MG has been reported.

Experimental

Materials: The methylglyoxal 40% solution, chitosan low molecular weight, polyamidoamine dendrimer generation 5.0 was purchased from Sigma Aldrich, USA. Microbiological media and ingredients were procured from HiMedia, India. All the other chemicals and biochemical were of analytical grade and purchased from Merck, Germany. Ultrapure Millipore water (18.2 MΩ) was used as solvent. *Escherichia coli* (MTCC 1687), *Pseudomonas aeruginosa* (MTCC 424), *Staphylococcus aureus* (MTCC 7405) and *Bacillus subtilis* (MTCC 441) were obtained from the Institute of Microbial Technology, Chandigarh, India. The bacterial strains were maintained on nutrient agar slants.

Synthesis of nanoformulated methylglyoxal: Methylglyoxal conjugated chitosan nanoparticles were prepared by emulsification crosslinking method. Briefly, 75 mg chitosan was dissolved in 50 mL of deionized water acidified with acetic acid and ultrasonicated for 30 minutes. Then 500 µl MG solution was added to the chitosan solution under stirring for another 30 minutes. Further, 750 µl of Tween 80 and 20% of sodium sufate solution have been added for emulsification and crosslink with chitosan particles. Finally, 50 µl of glutaraldehyde (10% in water) and 50 mg of sodium-metabisuphite was added to the above solution mixture and again stirred for 60 minutes. Hence, MG was conjugated with the amine group of chitosan nanoparticle. The solution was allowed to react at room temperature for 24 hours and dialyzed against the 0.9% saline water. The nanoformulated solution was transferred in a dialysis bag (cellulose acetate, MWCO =12 kDa) and immersed into water (100 mL). At appropriate time interval, 1 mL of the release media was taken and equivalent volume of fresh phosphate buffered saline (PBS) solution was supplemented in order to keep the volume of the system identical. The MG content can be determined by spectrophotometric analysis of MG derivatization reaction with high performance liquid chromatography (HPLC) analysis.[31] To a 1 ml sample containing methylglyoxal (0.5 to 10 µM), we added 0.2 ml of 5 M $HClO_4$, 0.1 ml of 10 mM 2,3-methylquinoxaline, 0.2 ml of 9.2 mM 1,2 diaminobenzene, and water to 2 ml final volume. Samples were incubated at room temperature (25°C) for 30 min and solid-phase extraction was performed in 5-mm 500-mg RP-18 columns activated with 2.5 ml methanol. After sample addition, the columns were washed twice with 2.5 ml 20 mM ammonium phosphate buffer of pH 2.3, and the samples were eluted. A spectrum was taken in the 400 to 800 nm range for MG concentration determination.

Further MG was loaded in the dendrimer matrix using an equilibrium dialysis method. The PAMAM dendrimer solution was dried under vacuum to remove methanol and dissolved in 1 mL deionized water. Then 50 µl MG solution was mixed with PAMAM-dendrimer and stirred overnight slowly in dark. Then the solution was transferred to a dialysis bag (MWCO 8000) and dialyzed twice against deionized water under strict sink conditions for 10 min to remove free MG. The encapsulation concentration of MG was determined by spectroscopic analysis. The average size and morphology of NMG and DMG were determined from TEM images. Particle size distribution and zeta potential of nanoformulated MG have been further characterized by Malvern Zetasizer Nano ZS instrument. In the *in vitro* release studies, 5 mL of both NMG and DMG were taken in a dialysis bag separately and were dialyzed under sink conditions. One mL of aliquots was collected after every 1h interval for 48 h and drug release was estimated indirectly using spectrophotometrically and double-distilled water as blank.

Antimicrobial Activity Evaluation: Antimicrobial activity of nanoformulated MG has been tested against *E. coli*, *P. aeruginosa*, *S. aureus*, and *B. subtilis* by broth dilution or agar-diffusion assay. The minimum inhibitory concentration (MIC) and minimum bactericidal concentration (MBC) of materials were determined using the broth micro dilution as well as a colony forming count method.

Hemolytic Activity: Toxicity to human red blood cells (RBCs) was assessed by a hemoglobin release assay. The assay stock, RBC was then mixed with each of the polymer based MG formulations of serial dilutions (10 µL) at a concentration of 0.04-100 µg/mL to give a final solution of 3% v/v RBC, which corresponds to approximately 10^8 red blood cells per mL based on counting in a hemacytometer. Buffer or Triton X-100 (1% v/v) was added as negative and positive hemolysis controls, respectively. The eppendrof were secured in a shaker at 37°C for 60 min and then centrifuged at 1000 rpm for 10 min. The absorbance at 450 nm was recorded using UV-Vis spectrophotometer. The percent of hemolysis was calculated as follows: Hemolysis % = [(sample absorbance−negative control)/ (positive control – negative control)] ×100%.

Cell culture: HeLa cells and Human fibroblast cells were obtained from National Center for Cell Science (NCCS), Pune (India), and maintained in DMEM medium supplemented with 10% FBS, 100 mg/L streptomycin and 100 IU/mL penicillin. The primary culture of the fetal mouse fibroblast was manipulated according to the regular processes. Cells were grown in 25 mL cell culture flask and incubated at 37°C in a humidified atmosphere of 5% CO_2 to approximately 70-80% confluence. Cells of 4-7 generations were used in this experiment.

Cytotoxicity assays (MTT assay): Human fibroblast cell line WI38 and Hela cells were used to determine the cytotoxicity of NMG. Cell toxicity was determined using MTT assay based on the reduction of a soluble tetrazolium salt by mitochondrial dehydrogenase of the viable cells to water insoluble colored product (i.e. formazan). The amount of the formazan produced proportional to the number of live cells. Reduction of the absorbance value can be attributed to the killing of the cells or inhibition of cell proliferation by the NMG. Briefly, WI38 and Hela cells were seeded at a density 2×10^5 cells per well in a 96-well microtiter plate for 12-24 h before the assay. The cells were incubated for 24 h at 37°C under 5% CO_2 in presence of varying concentration of NMG. Then, 50 µl of a 2 mg mL^{-1} MTT (Sigma; St Louis, MO) was added into each well, followed by 4 h of incubation at 37°C. The formazan crystals were then solubilized in 200 µl DMSO. The optical density (OD) at 570 nm was measured using an automated BioTek® Elisa Reader. The number of surviving cells was expressed as Percent viability = (The absorbance of the sample (treated cells)-background/the absorbance of the control (untreated cells)-background) × 100. Cellular toxicity of extracted contents from scaffolds was rated as follows: severe (<30%), moderate (30%–60%), slight (60–90%), or non-cytotoxic (>90%) of MTT activity, compared to the control cells cultured in extract-free medium.

SEM and TEM studies: The morphological changes of bacteria were treated with 0.8–8 µg/mL of NMG was investigated by Scanning Electron Microscopy (SEM) and Transmission Electron Microscopy (TEM). Aliquots of 20 µl of treated and untreated cell suspensions were deposited on glass cover slips. After being air dried for 1 h, the cover slips were fixed with a primary fixative solution containing 2.5% glutaraldehyde and 1% osmium tetraoxide. Subsequently, the cells were dehydrated with sequential treatment with 30, 50, 70, 80, 90, and 100% ethanol for 15 min. Finally, the cover slips were dried at room temperature and the cover slips were mounted on SEM stubs with carbon adhesive tabs and then sputter coated with a thin layer of gold. Digital images of the treated and untreated bacteria cells were acquired using a JEOL field emission scanning electron microscope (JSM-6700F) operating at an accelerating voltage of 5 kV. Transmission electron microscopy was carried out on JEOL JEM-2010 with an acceleration voltage of 200 kV.

Determination of potassium content: Exponentially growing *E. coli* cells were resuspended in 50 mM sodium Hepes buffer (pH 7.0) containing 5 mM glucose. After treatment with NMG, cells were washed and the cell pellets were digested with nitric acid. The potassium contents were determined by flame atomic emission spectroscopy (FAES) (Perkin-Elmer, 3110). Experiments were repeated thrice and mean was taken to plot the graph.

Cellular respiration assay: The triphenyl tetrazolium chloride (TTC) assay indirectly measures the microbial activity by assessing the electron transport system (ETS) activity using artificial electron acceptors, redox dyes that can successfully compete with oxygen for electrons (described in supporting information). Following a 12h treatment, the 96-well plate cultures with different concentration of NMG, the plates were again gently shaken and the absorbance at 490 nm was measured using a microplate reader. This assay is valuable in providing a reasonable estimation of bacterial respiration.

Cell Viability and Intracellular ROS Assays: The cell viability assay was based on the detection of cytoplasmic membrane damage based on the uptake of the fluorescent dye propidium iodide (PI). The nucleic acid-sensitive dye penetrates cells with compromised membranes while being expelled by healthy cells. The cellular oxidative stress assay employed the oxidative-reporter dye 5-(and-6)-carboxy-20, 70-dihydrodifluorofluorescein diacetate (H_2DCFDA). The cell-permeable H_2DCFDA is deacetylated by intracellular esterases which are readily oxidized by reactive oxygen species (ROS) forming the highly fluorescent DFF. NMG-exposed cultured cells were suspended in saline at 2×10^8 cfu mL^{-1} following removal of the excess NMG containing medium to avoid potential production of the fluorescent derivative DFFDA. The cell viability and cellular ROS assays were performed independently with 30 µM PI and 10 µM H_2DCFDA for 15 min and 2 h, respectively, at ambient temperature in the dark.

Microscopy Imaging: Following the staining process, cell samples were centrifuged for dye removal. Stained cells were visualized with a BX51WI fluorescence microscope (Olympus) equipped with 460-490 nm excitation filter setting and DP71 digital camera and DP-BSW software for image acquisition.

DNA binding assay: Plasmid DNA from *E. coli*, pBR322 was purified using Qiagen midi kit. The DNA was then quantified and the concentration was adjusted to100 ng/mL. The plasmid DNA was exposed to different concentrations of NMG to assess the *in vitro* interaction and effect of NMG on DNA structure and stability. The gel electrophoresis experiments were performed by mixing 100 ng of the plasmid DNA (pBR 322) with increasing amounts of NMG in presence of binding buffer (5% glycerol, 10mMTris–HCl, pH 8.0, 1 mM EDTA, 1 mM dithiothreitol, 20 mM KCl, and 50 µg/mL bovine serum albumin). Reaction mixtures were incubated at 37°C for 1 h. Subsequently, 4 µl of native loading buffer was added (10 mM Tris–HCl, pH 7.5, 50 mM EDTA, 0.25% bromophenol blue, and 0.25% xylene cyanol), and a 20 µl aliquot subjected to 0.8 % agarose gel electrophoresis in 0.5× Tris borate-EDTA buffer at 70 V (45 mM Tris-borate and 1 mM EDTA, pH 8.0).

Statistical analysis: Statistical analysis was performed using Origin 6 software. Each experiment was performed 3 to 5 times and results are expressed as mean ±SD and Student's t-test for significance was performed and $p<0.05$ was considered

significant. Cellular viability data show representative data of at least three independent experiments.

Results and Discussion

We have prepared small, highly dispersed nanoformulated MG in aqueous solution by using an emulsification mediated cross-linking method for chitosan polymer (Fig.1a). After 48 hours dialysis, the content of MG has been determined through spectroscopic technique. The average sizes of the NMG are estimated to be ~55 ±10 nm from transmission electron microscopy (TEM) images (Fig.1b).The NMG exhibit a spherical morphology without aggregation or adhesion (Inset: Fig.1b). At a fixed molar ratio, 1:2.6 [MG]: [polymer], NMG was obtained with an average hydrodynamic diameter of 68 ± 10 nm with a relatively narrow size distribution, as determined by dynamic light scattering (DLS) measurements (Fig.S1a). We have also synthesized another kind of nanoformulated MG via physical loading within the dendrimer polymer matrix using an equilibrium dialysis method (DMG) (Fig.1c). The DMG observed by TEM were approximately spherical in shape and 45 ± 5 nm in diameter which is consistent with their hydrodynamic radius as obtained from DLS measurement (Fig.1d and Fig.S1b). As the surface charge property of a material influences the biological activity, we have determined zeta potential of nanoformulated MG via electrophoresis measurement.[32] The NMG and DMG possess positive charge which depends on availability of amino functional groups of the polymers. The average size of nanoformulated MG prepared in the present study meet the size limit to be exploited *in vivo* drug delivery for encapsulated drug in polymeric nanocarrier. The percent entrapment of MG in NMG has been found to 82% ± 0.04 and for DMG ~91%±0.06. The loading efficiency also depends on concentration of polymers and MG, surface functional groups of the dendrimer molecules etc.

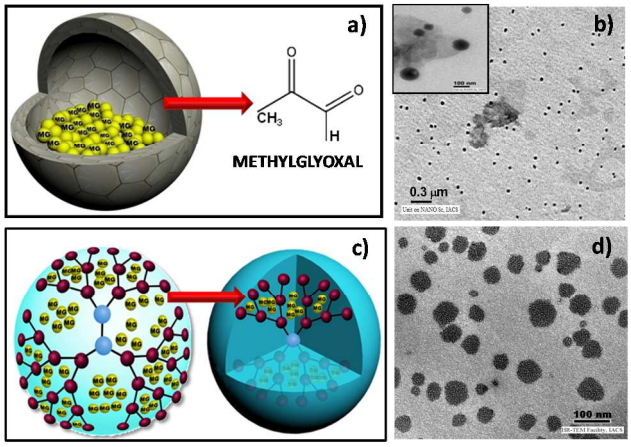

Fig.1 Schematic representation of polymer based nanoformulations of methylglyoxal (MG) and its characterization. (a) The structure of chitosan based nanoformulated methylglyoxal (NMG) showing methylglyoxal entrapped within the chitosan shell. (b) Transmission electron microscope (TEM) image of NMG. Inset: TEM image of NMG at high magnification. (c) The structure of dendrimer based nanoformulation of methylglyoxal (DMG). The MG molecules are physically encapsulated in the interior of dendrimer matrix. (d) TEM image of DMG.

To evaluate the release behaviour of MG from the polymer conjugates, we compared the performances of both chitosan and PAMAM dendrimers based nanoformulations (NMG & DMG). As shown in Figure 2, nearly more than 90% of MG molecules released out of the dialysis bag within 2 h in the absence of polymers.However, 75% of the MG released from PAMAM dendrimer after 12 h. Thus, G5 PAMAM dendrimer exhibits excellent capacity in the controlled release of MG owing to the construction of supramolecular structures between the cationic dendrimer surface (amino groups) and the two carboxylate groups in MG molecule. For the synthesized NMG, 43% of the MG molecules are released within 12 h. In comparison to the DMG, the slower releases of MG from NMG due to the presence of cross linking as well as hydrophobic, and hydrogen-bond interactions between chitosan and MG.

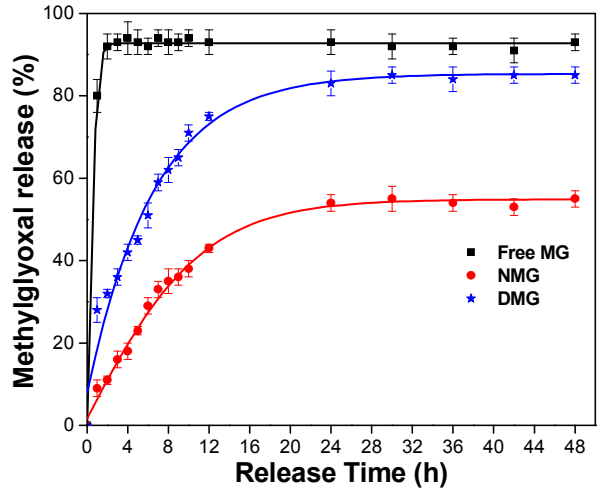

Fig.2 In vitro release studies (n=5). Values represent mean ±SD.

The antimicrobial activity of nanoformulations (NMG & DMG) was tested against four clinically significant micro-organisms both gram negative (*Escherichia coli, Pseudomonas aeruginosa*) and gram positive bacteria (*Staphylococcus aureus, Bacillus subtilis*). NMG have efficient broad spectrum antimicrobial activity against both gram positive and gram negative bacteria as demonstrated by effective zone of inhibition with decrease in order: *P. aeruginosa* > *S. aureus* >*B. subtillis* ≅ *E. coli*. However, DMG demonstrate sensitivity against gram negative bacteria *E. coli* and *P. aeruginosa* having a clear zone of inhibition (See Fig. S2 and Table S1). Thus, dendrimer based MG formulation is active against the gram-negative bacteria used in this study. NMG shows strong bactericidal activity with MIC ranging from 0.4 – 0.8µg/mL and MBC ranging from 1.6 – 2 µg/mL against gram positive bacteria (See Fig.S3). However, NMG shows activity with MIC ranging from 2 – 6 µg/mL and MBC 4 – 8 µg/mL against gram-negative bacteria, *P. aeruginosa* and *E. coli* respectively (See Fig.S4). Considering the MIC and MBC, *S. aureus* and *B. subtillis* are most susceptible to NMG, followed by *P. aeruginosa* and then *E. coli*. In contrast, DMG demonstrated strong bactericidal activity with MIC 0.8 µg/mL and MBC 1.6 – 2 µg/mL against *P. aeruginosa* and *E. coli*, respectively in comparison to MIC values of NMG. The differential antimicrobial efficiency for gram positive and gram negative bacteria is possibly due to the interaction between the negative charge of the bacterial outer membranes with NMG and DMG. The outer membranes of gram-negative and gram-positive bacteria are composed of lipopolysaccharides and teichoic acid respectively, which contribute the negative charge to the bacterial surface and consequently interact with the positive charge bearing nanoformulations.[33] Furthermore, higher cationic nature of DMG

with amine terminated dendrimer clearly contributes to their preferential recognition by the negatively charged outer surfaces of gram negative bacterial membranes. On the other hand, NMG have superior broad spectrum antimicrobial activity possibly allowing better penetration of MG due to chitosan mediated permeabilization to the bacterial cells.[34, 35] It may reasonably be assumed that chitosan molecule may contribute to the better effectiveness towards gram-positive bacteria and also sensitive towards gram negative bacteria. Furthermore, NMG shows concentration dependent bacterial growth inhibition in the broth medium by the measurement of optical density (O.D. at 600 nm) (See Fig.S5). This is consistent with the MBC value of NMG for *E. coli* by agar diffusion assay under similar conditions. It is well documented that chitosan polymer and bare MG have antimicrobial activity and for comparison the antimicrobial activity of pure chitosan and MG has also been evaluated by zone inhibition assay.[17,24] Interestingly, bare MG and chitosan with similar concentration used during the synthesis of nanoformulation have no significant effect on bacteria (See Fig. S6). Thus, the efficiency of NMG is not simply the sum of the efficiencies of pure chitosan polymer and MG rather the components shows antimicrobial activity synergistically. However, a serious impediment in biomedical application of dicarbonyl compounds being a normal metabolite, MG is prone to easy conversion to other metabolites resulting in substantially diminished efficacy of treatment. Earlier report suggested that biocidal activity of MG was demonstrated at concentration ≥1.05 mg/mL much higher concentration in comparison to nanoformulated MG.[17]A central premise of this work is the biological activity of MG could be augmented by encapsulating within the polymer in a more controlled fashion.

Our study aims to understand the cellular events that occur upon exposure to nanoformulated drugs with human blood. *In vitro* evaluation of NMG biocompatibility with human blood components is an essential test for early preclinical development as hemolysis i.e. destruction of red blood cells can further lead to anemia, jaundice, and other pathological conditions.[35] Interestingly, we observed that DMG has not induced any damage to red blood cells when tested *in vitro* at particular concentration range those effective towards bacteria (Fig.3 and See Fig.S7).

DMG exhibits high biocompatibility over a broad range of concentration adequate for potential pharmacological applications. However, with increasing the concentration of NMG causes a slight increase in the hemolytic activity. Less than 15% haemolysis has been observed at 64 µg/mL of NMG, a concentration much higher than the MBC, whereas DMG mediated 2.8 % hemolysis under the same conditions (Fig.3a). In fact, the HC_{50} value for both NMG and DMG could not be determined, having low levels of hemolytic activity which is significant for *in vivo* applications. According to several studies, *in vitro* hemolysis varies from 5 to 25% which has been regarded as non-toxic level[36] and our results meet the criteria of these studies.

Prior to evaluating NMG and DMG in living subjects, cytotoxic effects of nanoformulated MG against both human normal fibroblast cell line (WI38) and cervical cancer cell line (Hela) were examined in a MTT cell proliferation assay (MTT, 3-(4,5-dimethylthiazol-2-yl)2,5-diphenyl-tetrazoilum bromide). NMG did not showed significant cytotoxic effect up to 16 µg/mL concentration towards fibroblast cells, which has been found to be lethal for the bacteria tested in the present study (MBC 16 µg/mL, Table S2). Interestingly NMG was practically non-toxic for WI38 cells upto 8 µg/mL, since cell viability was higher than 90% (Fig.3b). This suggests that the NMG able to display strong antibacterial activity without being harmful to normal human fibroblast cells at bactericidal concentration.

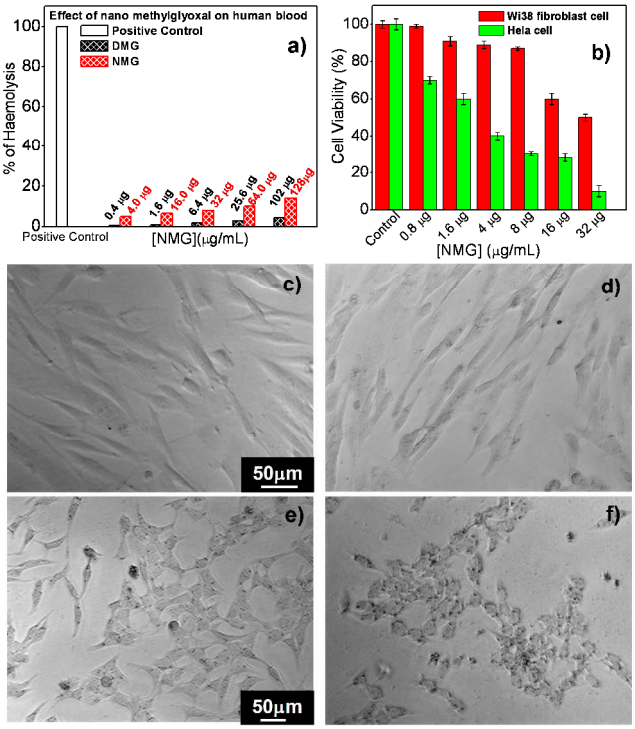

Fig. 3 Biocompatibility test of NMG on human blood. (a) Hemolysis assay for DMG and NMG using Triton-X as a positive control. (b) Cell viability of normal fibroblast cells (WI38) (red bar) and Hela cells (green bar) after 24-hours treatment with different concentrations of NMG as calculated from the MTT assay. The values are represented as mean SD of three individual experiments. Phase contrast images illustrating the overall cellular morphology of normal human fibroblast cells (WI38) without NMG (c), after 24 hrs incubation in presence of 32 µg/mL of NMG (d). Phase contrast images illustrating the cellular morphology of Hela cells without NMG (e), after 24 hrs incubation in presence of 32 µg/mL of NMG (f). The bar represents a scale of 50 µm.Data are the mean ± SD for three independent experiments.

In contrast, 8 µg/mL of NMG was highly toxic to Hela cells as cell viability is reduced by ~70% whereas ~90% of WI38 cell are viable at this concentration (Fig.3b). To examine the cytotoxic effect on the morphology of WI38 and Hela cells, cells were treatment with varying concentrations of NMG. The data indicate the cell viabilities for each cell type normalized to a control cell sample that was not incubated with any nanoformulated MG (Fig.3c and 3e). Phase contrast microscopic observations showed no distinct morphological changes in the WI38 cells treated with upto 8 µg/mL NMG and the trypan blue exclusion method also indicated more than 95% cell viability (data not shown) indicating healthy cells at the bactericidal concentration. But, significant decrease in WI38 cell viability has been observed at much higher concentration (32 µg/mL) (Fig.3d). However, NMG showed significant toxicity towards Hela cells as evident from microscopic observations which also support the result as determined by MTT assay where less than 10% cells have been

found to be viable after treatment with 32 µg/mL NMG (Fig.3a) and further confirmed by trypan blue exclusion assays (data not shown). Microscopic observations of the treated HeLa cells showed distinct morphological changes where the cells have a tendency to become rounded and form aggregate. The intercellular connectivity also decreased after treated with NMG. This suggests that immobilization of MG in the polymer matrix can exert anticancer activity but has no cytotoxic effect on normal mammalian cells. In previous report, it has been found that MG has selectively inhibitory effect on mitochondrial complex I of malignant cells without affecting the normal cells.[37, 38] This might be feasible explanation for cytotoxicity of NMG towards Hela cells.

To better understand the cellular specificity of nanoformulated MG displayed in the above experiment, we have calculated therapeutic index (TI) which is widely accepted as measurement of cell selectivity of antimicrobial agents.[39] A larger therapeutic index indicates greater cellular selectivity. The TI of the NMG and DMG was calculated as the ratio of the lowest concentration that produces 10% haemolysis (MHC) value to the geometric mean (GM) of MICs against selected microorganisms (Table S2). Since there is no significant hemolysis at the highest tested concentration for DMG, 102 µg/mL was used for the TI calculation. DMG displayed much higher cell selectivity (more than 3-fold increased) as compared to NMG due to high hemocompatibility (Table S2). Since NMG is non-hemolytic at its bactericidal concentration, we have followed up further study on mechanistic aspects antimicrobial activity of NMG against bacteria cells.

The direct influence of NMG on the structural integrity of bacteria has been visualized by both scanning electron microscopy (SEM) and transmission electron microscopy (TEM). NMG concentrations are chosen based on their MIC and MBC data (Table S2) in order to obtain a comparable killing rate. One representative gram negative strain, *P. aeruginosa* and gram positive strain, *B. subtilis* have been exposed to the NMG at sub-MICs and MBC for microscopic image (Fig.4). Untreated bacteria cells display a rough bright surface with no apparent cellular debris (Fig. 4a and 4d). In contrast, morphological alterations of bacterial cells after exposure with MIC and MBC concentrations of NMG exhibit significant abnormalities with cellular aggregation, shrinkage and depression of cell wall.

After incubation with the lethal concentration (MIC) of NMG (Fig.4b and see S8b), the majority of the gram negative cells have been found to be highly aggregated with compromised outer membrane structure (marked with green doted circle). On having closer look, *P. aeruginosa* cells in presence of MIC of NMG clearly shows NMG are strongly attached to the surface of bacteria (marked with red dotted square, Fig. 4b). However, in presence of killing concentration (MBC) of NMG, the majority of the *P. aeruginosa* cells have lost their cellular integrity and become elongated or flattened, indicating irreversible cell damage or cell death (Fig. 4c and S8c) compared to the untreated cells (Fig. 4a and S8a). However, the majority of the gram positive bacterial cells after exposure to the NMG (Fig. 4d-f and S8d-f) exhibits notable alterations in the cell membrane and the cell wall leading to loss of cellular integrity and loss of cytoplasmic contents even at MIC concentration. After treatment of *S. aureus and B. subtilis* with a MIC of NMG, we found most of the bacteria have burst with deep craters in their cell wall (Fig. 4e and S8e), while at a MBC numerous lysed cells and cell debris are observed (Fig. 3f and S8f) compared to control cells (Fig. 3d and S8d). The gram positive bacteria cells are more sensitive to the NMG.

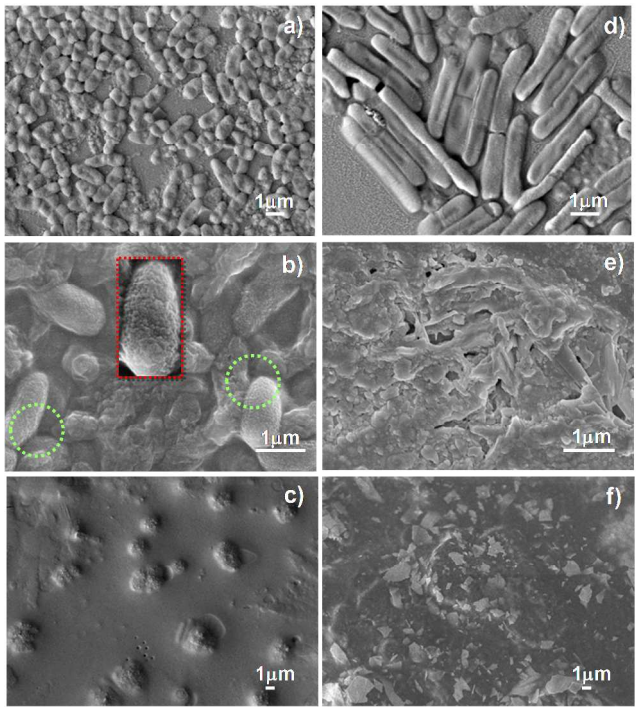

Fig. 4 SEM images of *P. aeruginosa* untreated (a), *P. aeruginosa* treated with MIC of NMG (b), and MBC of NMG (c) respectively. The bacterial aggregation is marked with dotted green circles and surface adsorption of NMG on bacteria is marked with red dotted box. (d) *B. subtilis* untreated, (e) *B. subtilis* treated with MIC of NMG and (f) *B. subtilis* treated with MBC of NMG respectively.

In general, gram-negative bacteria are more resistant to antibiotics than gram-positive bacteria due to having a complex outer membrane.[40] The complex outer membrane of gram-negative bacteria may have enhanced their surface stiffness which may contribute higher resistance to physical perforation by NMG, which would result in the bacterial death at higher MBC compared with gram positive bacteria (Table S1). The morphological changes of cells and the internalization of NMG have been further examined by TEM images (Fig. S9). The remarkable morphological alterations of bacterial cells have also been visualized in TEM images. At MIC of NMG, a more frequent and prominent collapse of the cell structure is noticeable and the cells seemed to have lost their content, although the overall cell shape is still recognizable (Fig. S9 a-f). This is also in agreement with the SEM image. TEM micrographs of control P. *aeruginosa* and *B. subtilis* shows rod shape cells with intact cell walls and well-defined membranes (See Fig. S10 and S11). The intracellular DNA region displays a heterogeneous electron density. However, after treated with NMG, the cytoplasm reveals a more uniform electron density (Fig. S9a). Additionally, *P. aeruginosa* cell shows leakage in the cellular membrane (indicated by red box in the micrographs) followed by an outflow

of the cytoplasmic component as shown in Fig. S9b. Moreover, both at MIC and MBC of NMG, we observe cell lysis and large amount of cellular debris around the cell (marked by red arrow in the TEM micrographs). These suggest that the extent of membrane damage increases with increasing NMG concentration, until a significant disruption of the membrane structure occurs, followed by death of the bacteria cell. The TEM image of *B. subtilis* cells confirms the presence of NMG in the cell membrane and inside the bacterial cells which cause permeabilizations of the both outer and inner membrane that finally lead to the leakage of cytoplasmic contents as evident (marked by white arrow, Fig. S9c-e). Chitosan molecules can directly interact with bacterial cells based on the interaction between positively charged chitosan molecules and negatively charged microbial cell membranes which may cause membrane permeabilization.[41] Consequently, chitosan encapsulated MG are easily enter into the bacteria cell having strong antimicrobial action. Interestingly, at a sub lethal NMG concentration (MIC), the inner membrane becomes permeable to small compounds, but at this stage the bacteria are still alive. Instead, at a high NMG concentration, the membrane becomes leaky to large cytoplasmic components, which is concomitant with death of bacteria. Therefore it is reasonable to speculate that at high NMG concentration, a rapid killing occurs owing to a severe loss of membrane integrity. The extensive loss of cell membrane structure suggests that the NMG not only perturbed the cell membrane but may have also chemically degraded or oxidized the membrane.

Furthermore, the oxidative stress-based signaling mechanism may be reciprocated by nanoparticles through the generation of reactive oxygen species (ROS) in living cells, including bacterial cells is often taken as a measurement of cytotoxicity.[42] Compared with the control bacteria, rapid intracellular reactive oxygen species (ROS) generation in bacteria cells has been followed by the H_2DCFDA staining within one hour of exposure to NMG (1µg/mL) with further increase in concentration of NMG (at MIC and MBC, 6 and 8 µg/mL) significantly promoting ROS generation (Fig. 5a-c).

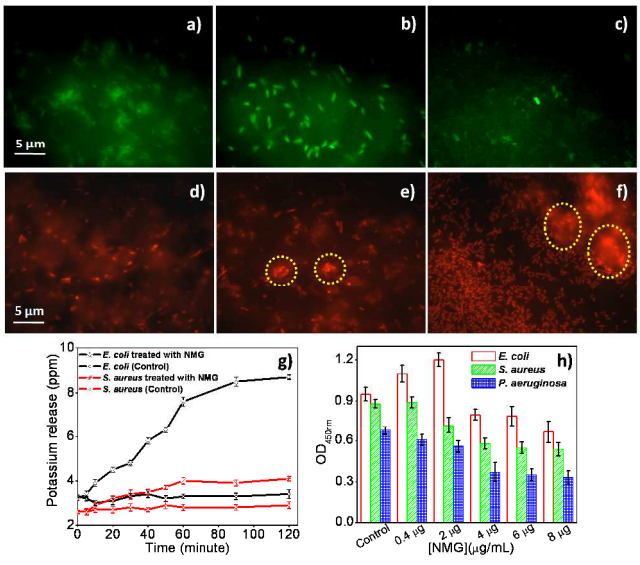

Fig. 5 The detection of NMG mediated intracellular ROS generation (H_2DCFDA staining, green) and cell death (PI staining, red) of *E. coli* stain by fluorescence microscopy. All stained samples were imaged at comparable cell concentration. Microscopy images show ROS generation when *E. coli* treated with (a) 1 µg/mL, (b) 4 µg/mL and (c) 8 µg/mL of NMG. Microscopy images show PI staining when *E. coli* treated with (d) 1 µg/mL (e) 4 µg/mL (f) 8 µg/mL of NMG. NMG induced cellular aggregation and cell lysis due to damage of cellular membrane is highlighted with yellow circle. Microscopy images were obtained with 100X magnifications in a Carl Zeiss Axio Observer Z1 Fluorescence microscope. (g) Determination of cellular potassium content of log phase E. coli and S. aureus after treated with NMG at room temperature by flame atomic emission spectroscopy (FAES) at various time intervals. K^+ ion efflux in untreated control cells were also monitored to compare with the potassium release on exposure to NMG. Experiments were repeated thrice. (h) Effect of NMG on the metabolic activity of bacteria cells by respiration assay.

Additionally, the cell viability of NMG treated bacterial cells showing ROS generation also has been studied using propidium iodide (PI) staining as shown in Fig. 5d-f. The higher proportion of PI-positive cells after treated with increasing concentration of NMG relative to the control implies the cytoplasmic membrane as one of the target destruction sites of the NMG-induced ROS as microscopic images have demonstrated severe membrane damages. The control bacteria in absence of NMG show well dispersed structure without aggregation, ROS generation and less PI staining (Fig. S12 a-c). Another aspect to consider for the understanding of the mechanistic basis of the membrane-permeabilizing action of the NMG that may affect the osmo-regulatory capacity of the bacteria even at low (sub-MIC) concentrations leads to cell lysis.[43-45] Fig. 5g illustrates leakage of potassium ions from *E. coli* and *S. aureus* in the presence of NMG at their respective MICs. NMG induces leakage of potassium ions from *E. coli* cells as evident from the sharp increase in K^+ ion efflux in a time dependent manner where more than 2.5 -fold K^+ ion efflux observed compared to that of control after an hour of treatment. However, in comparison to *E. coli*, efflux from *S. aureus* cells has been found to continue at a slower rate, reaching >1.5 times after 120 min. Differences in the susceptibility of the test organisms to NMG are also observed possibly due to variations in the rate of penetration of NMG through cell wall and cell membrane structures. It is conceivable that this loss of intracellular potassium may disrupt the permeability barrier of cell membrane structures which is well documented in earlier report.[44] Along the line of concept, the bacterial cytoplasmic membrane provides a permeability barrier to the passage of small ions such as H^+, K^+, Na^+ and Ca^{2+} which is regulated by the structural and chemical composition of the membrane structure. Additionally, preservation of ion homeostasis is vital process to control the energy status of the cell as well as membrane-coupled energy-dependent processes such as solute transport, regulation of metabolism etc.[45] So, increases in the leakage of K^+ will indicate a disruption of this permeability barrier and even relatively small changes to the structural integrity of cell membranes can detrimentally affect cell metabolism and lead to cell death. The membrane permeability by NMG in microbial cells suggests that their antimicrobial action is primarily the result of inhibition of membrane-located metabolic events and a loss of chemiosmotic control. The inhibition of respiration also accompanied by the increased cell membrane permeability and we have followed the effects of NMG on respiration of bacteria cells. Fig. 5h demonstrates a significant inhibition of metabolic activity of bacterial cells obtained upon exposure to NMG. The biological reduction of

tetrazolium salts has been correlated with electron transport system (ETS) activity in respiring cells and thus used as an index of metabolic activity.[46, 47] The reduction of 2, 3, 5-Triphenyl tetrazolium chloride (TTC) by metabolically active cells forming purple color complex indicates the level of metabolic activity (Fig. S13). Regulation of the respiratory ETS can be accomplished by a change in enzyme activity of the ETS enzymes and permits fine tuning of respiration in response to rapidly changing environmental or intracellular conditions.[48] Moreover, the respiratory electron transport activity was closely correlated with oxygen consumption in aerobic bacterial cultures. NMG inhibited respiration of cell suspensions of *E. coli*, *S. aureus* and *P. aeruginosa* as shown in Fig. 5h. Inhibition of *E. coli* respiration increases with increasing the concentration of NMG. Finally, at bactericidal concentration (8 µg/mL), 30% inhibition has been observed for *E. coli*. Respiration in *S. aureus* cells is also inhibited by 35% at a NMG concentration corresponds to the MBC (2 µg/mL) for this organism. The viability of *P. aeruginosa* decreases rapidly with 45% inhibition of respiration in presence of 4 µg/mL of NMG. The relative inhibition of respiration and the extent of membrane damage of these micro-organisms as evident from microscopic image follow the same pattern. Such perturbation in cellular metabolism causes the formation of lethal hydroxyl radicals.[49] However, *B. subtilis* does not show significant change in metabolic activity in presence NMG compared to the control microorganism. Considering the broad spectrum activities of NMG towards both gram positive and gram negative bacteria with membrane-damaging effect, it is expected that this variability reflects the rate at which its active components diffuse through the cell wall and into the phospholipids region of cell membrane structures. This finding suggests that the potential bioactive NMG have distinct influence on bacteria cell metabolism depending on the cell membrane structure.

Further, we have investigated the effect of NMG on DNA of cells through 4, 6-diamidino-2-phenylindole (DAPI) staining. The fluorescent microscopic studies after DAPI staining of untreated Hela cells does not show any fragmentation (Fig. 6a) and the corresponding DIC image also shows well-shape healthy cells (Fig. 6b). However, NMG treated HeLa cells clearly exhibit nuclear fragmentation (Fig. 6c) and the DIC images corroborate the cellular damage (Fig. 6d). We have also shown the nuclear fragmentation at higher magnification (at 100X) which are highlighted with dotted yellow box (Fig. 6e) and overlay of fluorescence (Fig. 6f) and bright field image of the corresponding image (Fig. 6g). This suggests the potential cytotoxicity of NMG towards cancer cells via DNA degradation. Additionally, the plasmid DNA model is a relatively simple system that allows the study of NMG induced DNA damage using agarose gel electrophoresis.[50] The plasmids are double stranded extra chromosomal DNA whose sizes ranges from a few hundred to a few thousand base pairs in length and are normally present in bacteria. The effect of NMG on plasmid DNA isolated from *E. coli* (pBR322) has been tested by treating the DNA with NMG of gradually increasing concentrations ranging from 0.4-8 µg/mL for 60 minutes at 37°C in phosphate buffered saline (PBS) maintained at pH 7.4. After the incubation, the fate of DNA has been analyzed by agarose gel electrophoresis (Fig. 6h). The untreated DNA shows single band as supercoiled form (lane i). The polymer chitosan (1.5 mg) and bare MG (8 and 64 µg/mL) were also incubated with DNA as controls and none of these components are able to degrade DNA. We observe NMG induced DNA degradation and the degree of DNA degradation is directly proportional to the concentration of NMG as shown in Fig. 6h, lanes v-ix. Generally, the plasmid exists as a double stranded covalently closed circular DNA having supercoiled conformation which makes the plasmid smaller in size and thus migrates faster through the gel pore. However, once a strand of the double helix is damaged by free radicals generated by nanomaterials, plasmid becomes an open-circular or relaxed molecule. The relaxed conformation moves slower in agarose gel electrophoresis indicating DNA damage upon exposure to NMG. The smear like appearance in the lanes loaded with DNA which were treated with different concentration of NMG indicates DNA degradation depending on NMG concentration.

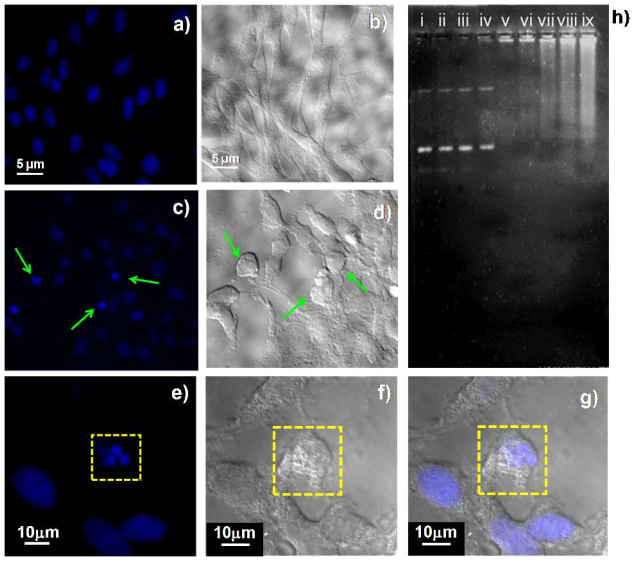

Fig.6 Cytotoxic effect of NMG on Hela cells. (a) Fluorescence microscopic images of DAPI stained untreated Hela cells and (b) phase contrast microscopic images of untreated Hela cells. (c) Fluorescence microscopic images of DAPI stained Hela cells treated with NMG, (d) phase contrast microscopic images of Hela cells treated with NMG. Green arrows indicate fragmented nuclei. (e) Fluorescence microscopic images of DAPI stained Hela cells treated with NMG at different magnification where fragmented nuclei is marked with dotted yellow box, (f) phase contrast microscopic images of Hela cells treated with NMG at different magnification where fragmented nuclei is marked with dotted yellow box. (g) Overlay of fluorescence and bright-field microscopy images of Hela cells treated with NMG. The scale bar is 10 µm. DNA fragmentation was analyzed by electrophoresis on a 1.6% Tris-Borate-EDTA agarose gel. (h) The in vitro effect of NMG on plasmid DNA. Lane (i): Negative control-untreated DNA, Lane (ii): DNA treated with chitosan polymer (1.5 mg), Lane (iii-iv): DNA treated with bare MG of 8 and 64 µg/mL, Lane (v): DNA treated with 0.4 µg/mL of NMG, Lane (vi): DNA treated with 0.8 µg/mL of NMG, Lane (vii): DNA treated with 1.6 µg/mL of NMG, Lane (viii): DNA treated with 4 µg/mL of NMG. Lane (ix): DNA treated with 8 µg/mL of NMG.

On the basis of the experimental results described here, we propose a mechanism of the antimicrobial activity of NMG that involves both the surface binding and a ROS-dependent pathway, as shown in scheme 1. A series of steps, cell responses and interactions as well as intervention of cellular processes may

possibly be involved during inhibition of bacterial growth.[51] Most of the ROS products derived from sequential univalent reductions of molecular oxygen catalyzed by several membrane–associated respiratory chain enzymes. Experimental data suggest that, the respiratory chain can account for ~87% of the total H_2O_2 production in *Escherichia coli*.[52] The leakage of single electrons from the bacterial respiratory chain was observed at the NADH dehydrogenase which was similar to that observed in eukaryotic mitochondria.[53] In fact, free radicals can attack directly polyunsaturated fatty acids in membranes which alters membrane properties and can disrupt membrane-bound proteins significantly. This effect acts as an amplifier and more radicals are formed. Thus, lipids are also major targets during oxidative stress and we studied the membrane leakage by determining the release of Na and K ions. Additionally, excessive accumulation of MG may induce modifications of mitochondrial proteins leading to dysfunction of the mitochondria and increases in the production of reactive oxygen species (ROS).[54]

In the first step, the NMG can interact with the negatively charged bacterial surface of the outer membrane consisting of the anionic lipopolysaccharide and permeation followed by binding to the anionic inner membrane through electrostatic and hydrophobic interactions which finally leads to disruption of these membranes. The mechanism may be the oxidative stress through which NMG may suspend different cellular process and –or affect cellular structures which causes cellular disintegration and cell death. The mechanism is supported by SEM images of bacteria in contact with NMG displaying significant loss of cell membrane structure (Fig. 4 and 5).

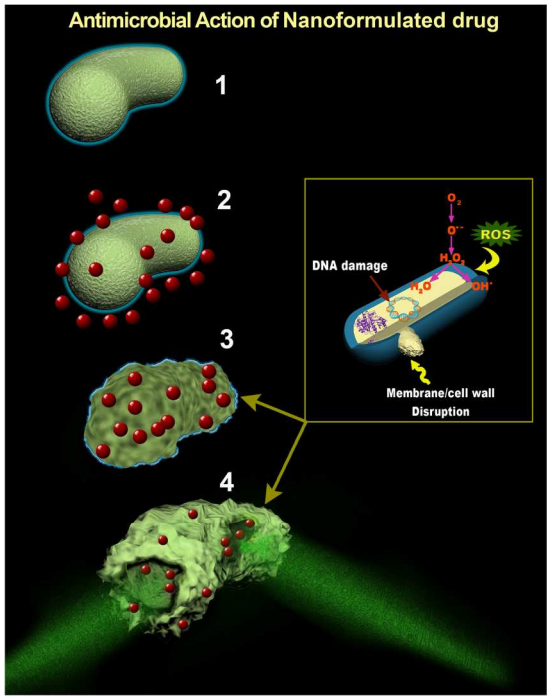

Scheme 1. The proposed mechanism of antimicrobial activity of NMG. Here 1 to 4 represents mechanistic steps of antimicrobial action of NMG. 1. Control bacteria without treatment of NMG, 2. Closer approach of NMG to the bacterial surface after treatment, 3. Cellular uptake of NMG with compromised membrane integrity, 4. Cellular burst happened with structural damage of bacteria.

In next step, the NMG can enter into the bacterial cells, attack the respiratory chain inhibiting one or more respiratory enzymes, facilitates the generation of reactive oxygen species which have adverse effects on cellular macromolecules and cellular organelles and consequently causes damage to DNA molecule to become fragmented leading to cell death.[55] As highly reactive dicarbonyls of MG molecule can attack the lysine, arginine (Arg) and cysteine residues of proteins and also DNA synthesis.[56] It can be assume that NMG directly inhibits a specific respiratory enzyme or metabolic pathway via the oxidation of the reducing cellular energy carriers like NADH and NADPH (Fig. 4) and leakage of potassium ions commenced upon exposure of NMG may alter cell membrane structure. Previously, Cox *et al*. have shown that tea tree oil inhibits respiration and causes leakage of cellular potassium in *E. coli* which in turn damages cell membrane structure.[57]

Generally, the cytoplasmic membranes and plasma membranes of bacteria provide a barrier to the passage of small ions such as H^+, K^+, Na^+ and allow controlling the entry and exit of different compounds within the cells and organelles, respectively. This permeability barrier play important role to maintain cellular functions, including the management of the energy status of the cell, other membrane-coupled energy-transducing processes, solute transport, and regulation of metabolism.[58] Furthermore, it has been proposed that reactive oxygen species can induce apoptotic pathways in bacteria and then DNA gets fragmented ultimately leading to cell death. The DNA fragmentation could be visualized in agarose gel after plasmid DNA has been treated with NMG (Fig. 6h). These findings along with the microscopic images indicate a three-step antimicrobial mechanism which includes initial cell deposition of NMG on bacterial surface, membrane stress caused by direct contact with NMG, and the ensuing superoxide anion-dependent oxidation and DNA damage.

Conclusions

In summary, we have developed a simple, nontoxic, water-based synthetic methodology for the synthesis of multifunctional polymer conjugated nanoformulations of MG by soft chemistry. We have demonstrated that the nanoformulated MG are effective antimicrobial agents for the selective killing of pathogenic bacteria. Our results suggest that these materials have quite promising applicability against drug-resistant bacteria with low MIC values, yet induce relatively low hemolysis. The conjugation of MG with polymer in nano dimension strongly enhances bioactivity of bulk MG. In addition, these materials have a high therapeutic index against bacterial infection. Importantly, they do not cause toxicity to normal human fibroblast cell, indicating that these nanoformulated MG may provide an efficient antimicrobial agent in treating bacterial infections. We have observed that the NMG mediated superoxide generation causes an elevated role of oxidative stress, inhibition of cellular respiration and potassium ion leakage leads to increase membrane permeability and allowing better penetration of MG into the cell. Mechanistically, it appears that permeabilization of the outer bacterial membrane by chitosan nanoparticles enhances the intrinsic antibiotic effect of the MG minimization of environmental release through excess ion production of nanoparticles beyond that necessary for product

performance. Thus, the present investigation opens up the possibility of exploring the conjugation of polymer nanoparticles with MG for the treatment of bacterial infections with minimal cytotoxicity. The novel approach of identifying chemical scaffolds leads to a new generation antimicrobial agents which can target a spectrum of pathogens and overcome resistance due to multimodal activity.

Acknowledgements

Financial support under Grant #SR/S5/NM-47/2005 and Grant# SR/NM/NS-49/2009 from DST, India are gratefully acknowledged. S.G. and M. R. gratefully acknowledge the Council of Scientific and Industrial Research, India for financial support. The authors thank Prof. S. Ghosh, Ballygunge Science College, kolkata for providing superoxide measurements in bacterial cells.

Notes and references

1. K. E. Jones, N. Patel, M. Levy, A. Storeygard, D. Balk, J. Gittleman and P. Daszak, *Nature*, 2008, **451**, 990–993.
2. A. J. Lax, *Nat. Rev. Microbiol.,* 2005, **3**, 343–349.
3. M. Kamboj and K. A. Sepkowitz, *Lancet Oncol*., 2009, **10**, 589–597.
4. M. J. Hill, *Eur J. Cancer Prev.*, 1995, **4**, 127–128.
5. M. N. Alekshun and S. B. Levy, *Cell*, 2007, **128**, 1037–1050.
6. G. D. Wright, *Nat. Rev. Microbiol.,* 2007, **5**, 175–186.
7. L. M. Weigel, D. B. Clewell, S. R. Gill, N. C. Clark, L. K. McDougal, S. E. Flannagan, J. F. Kolonay, J. Shetty, G. E. Killgore and F. C. Tenover, *Science*, 2003, **302**, 1569–1571.
8. D. Banerjee and D. Stableforth, *Drugs*, 2000, **60**, 1053–1064.
9. N. Woodford and D. Livermore, *J. Infect.*, 2009, **59**, S4–S16.
10. W. B. Hugo and A. D. Russell, Types of antimicrobial agents. In: Principles and practice of disinfection, preservation and sterilization. Oxford, UK: Blackwell Scientific Publications; 1982, pp. 106–108.
11. M. Adolfsson-Erici, M. Pettersson, J. Parkkonen and J. Sturve, *Chemosphere*, 2002, **46**, 1485–1489.
12. A. Kumar, P. K. Vemula, P. M. Ajayan and G. John, *Nat. Mater.*, 2008, **7**, 236–241.
13. Q. Li, S. Mahendra, D. Y. Lyon, L. Brunet, M. V. Liga, D. Li and P. J. J. Alvarez, *Water Res.*, 2008, **42**, 4591–4602.
14. M. L. Schipper, N. Nakayama-Ratchford, C. R. Davis, N. W. S. Kam, P. Chu, Z. Liu, X. Sun, H. Dai and S. S. Gambhir, *Nat. Nanotechnol.,* 2008, **3**, 216–221.
15. P. V. AshaRani, G. L. K. Mun, M. P. Hande and S. Valiyaveettil, *ACS Nano,* 2009, **3**, 279–290.
16. R. Duncan, *Nat. Rev. Cancer,* 2006, **6**, 688–701.
17. E. Mavric, S. Wittmann, G. Barth and T. Henle, *Mol. Nutr. Food Res.*, 2008, **52**, 483–489.
18. L. G. Együd and A. Szent-Györgyi, *Science*, 1968, **160**, 1140.
19. D. Talukdar, S. Ray, M. Ray and S. Das, *Drug Metabol. Drug Interact.,* 2008, **23**, 175–210.
20. A. Pal, I. Bhattacharya, K. Bhattacharya, C. Mandal and M. Ray, *Mol. Immunol.*, 2009, **46**, 2039–2044.
21. C. A. De Bock, J. Brug and J. N. Walpo, *Nature,* 1957, **179**, 706–707.
22. J. Haldar, D. An, L. A. de Cienfuegos, J. Chen and A. M. Klibanov, *Proc. Natl. Acad. Sci. USA*, 2006, **103**, 17667–17771.
23. E. R. Kenawy, S. D. Worley and R. Broughton, *Biomacromolecules,* 2007, **8**, 1359–1384.
24. Y. Lu, D. L. Slomberg and M. H. Schoenfisch, *Biomaterials*, 2014, **35**, 1716–1724.
25. Y. Guo, M. Chu, S. Tan, S. Zhao, H. Liu, B. O. Otieno, X. Yang, C. Xu and Z. Zhang, *Mol. Pharmaceutics*, 2014, **11**, 59–70.
26. D. A. Tomalia, A. Nayor and W. I. Goddard, *Angew. Chem. Int. Ed. Engl.*, 1990, **29**, 138–175.
27. E. R. Gillies and J. M. J. Réchet, *Drug Discovery Today*, 2005, **10**, 35–43.
28. Y. Lu, D. L. Slomberg, A. Shah and M. H. Schoenfisch, *Biomacromolecules*, 2012, **13**, 3343–3354.
29. Y. Lu, D. L. Slomberg, A. Shah and M. H. Schoenfisch, *Biomacromolecules*, 2013, **14**, 3589–3598.
30. S. H. Medina and M. E. H. El-Sayed, *Chem. Rev.,* 2009, **109**, 3141–3157.
31. S. Hara, M.Yamaguchi, Y. Takemori, T. Yoshitake, and M. Nakamura, *Anal. Chim. Acta*, 1988, **215**, 267–276.
32. S. Ghosh, D. Ghosh, P. K. Bag, S. C. Bhattacharya and A. Saha, *Nanoscale*, 2011, **3**, 1139–1148.
33. M. Stark, L. Liu and C. M. Deber, *Antimicrob. Agents Chemother*., 2002, **46**, 3585–3590.
34. N. G. M. Schipper, K. M. Varum, P. Stenberg, G. O. Cklind, H. Lennernas and P. Artursson, *Eur J. Pharm Sci.,* 1999, **8**, 335–343.
35. M. A. Dobrovolskaia, J. D. Clogston, B. W. Neun, J. B. Hall, A. K. Patri and S. E. McNeil, *Nano Lett.,* 2008, **8**, 2180–2187.
36. K. Amin and R. M. Dannenfelser, *J. Pharm. Sci.,* 2006*,* **95**, 1173–1176.
37. S. Patra, A. Ghosh, S. S. Roy, S. Bera, M. Das, D. Talukdar, T. Wallimann and M. Ray, *Amino Acids,* 2012, **42**, 2319–2330.
38. M. Ghosh, D. Talukdar, S. Ghosh, N. Bhattacharyya, M. Ray and S. Ray, *Toxicol. Appl. Pharmacol.*, 2006, **212**, 45–58.
39. Y. Chen, C. T. Mant, S. W. Farmer, R. E. Hancock, M. L. Vasil and R. S. Hodges, *J. Biol. Chem.,* 2005, **280**, 12316–12329.
40. D. Voet, J. G. Voet and C. W. Pratt, Fundamentals of Biochemistry; John Wiley & Sons, Inc.: New York, 2006.
41. S. Senel, G. Ikinci, S. Kaş, A. Yousefi-Rad, M. F. Sargon and A. A. Hincal, *Int. J. Pharm.,* 2000, **193**, 197–203.
42. R Zhang, Y. J. Niu and Y. K. Zhou, *Toxicol. Lett.,* 2010, **192**, 108–114.
43. N. Geerts, T. Schmatko and E. Eiser, *Langmuir,* 2008, **24**, 5118–5123.
44. F. M. Campos, J. A. Couto, A. R. Fig.ueiredo, I. V. Tóth, A. O. Rangel and T. A. Hogg, *Int. J. Food Microbiol.,* 2009, **135**, 144–151.
45. S. Tachon, D. Michelon, E. Chambellon, M. Cantonnet, C. Mezange, L. Henno, R. Cachon and M. Yvon, *Microbiol.*, 2009, **155**, 2941–2948.
46. B. L. Trumpower and R. B. Gennis, *Annu. Rev. Biochem.,* 1994, **63**, 675–616.
47. D. T. Vistica, P. Skehan, D. Scudiero, A. Monks, A. Pittman and M. R. Boyd, *Cancer Res.,* 1991, **51**, 2515–2520.
48. A. M. Dean and D. E. Jr. Koshland, *Science,* 1990, **247**, 1044–1046.
49. M. A. Kohanski, D. J. Dwyer and J. J. Collins, *Nat. Rev. Microbiol.,* 2010, **8**, 423–435.
50. Y. Zheng and L. Sanche, *Radiat. Res.,* 2009, **172**, 114–119.
51. C. Walsh, *Nature*, 2000, **406**, 775–781.
52. B. González-Flecha and B. Demple, *J. Biol. Chem.,* 1995, **270**, 13681–13687.
53. S. Ghosh, M. Ray, M. Das, A. Chakrabarti, A. H. Khan, D. D. Sarma and S. Acharya, *Phys. Chem. Chem. Phys.,* 2014, **16**, 5276–5283.
54. J. Halder, M. Ray and S. Ray, *Int. J. Cancer*, 1993, **54**, 443–449.
55. Y. Matsumura, K. Yoshikata, S. Kunisak and T. Tsuchido, *Appl. Environ. Microbiol.*, 2003, **69**, 4278–4381.
56. Y. Midorikawa, H. Hibasami, P. Gasaluck, H. Yoshimura, A. Masuji and K. M. Nakashima Imai, *J. Appl. Microbiol.,* 2008, **70**, 291–293.
57. S. D. Cox, J. E. Gustafson, C. M. Mann, J. L. Markham, Y. C. Liew, R. P. Hartland, H. C. Bell, J. R. Warmington and S. G. Wyllie, *Lett. Appl. Microbiol.*, 1998, **26**, 355–358.
58. B. Poolman, A. J. M. Driessen and W. N. Konings, *Microbiol. Rev.,* 1987, **51**, 498–508.